Correlation Between Processing Conditions, Microstructure and Mechanical Behavior in Regenerated Silkworm Silk Fibers

Gustavo R. Plaza,[1] Paola Corsini,[2] Enrico Marsano,[2] José Pérez-Rigueiro,[1] Manuel Elices,[1] Christian Riekel,[3] Charlotte Vendrely,[3] Gustavo V. Guinea[1]

[1]Departamento de Ciencia de Materiales, ETSI Caminos, Canales y Puertos, Universidad Politécnica de Madrid, Madrid 28040, Spain

[2]Dipartimento di Chimica e Chimica Industriale, Università di Genova, Via Dodecaneso Genova 31-16146, Italy

[3]European Synchroton Radiation Facility, B.P. 220, F-38043, Grenoble Cedex, France

Correspondence to: J. Pérez-Rigueiro (E-mail: jperez@mater.upm.es)

ABSTRACT: Regenerated silkworm fibers spun through a wet-spinning process followed by an immersion postspinning drawing step show a work to fracture comparable with that of natural silkworm silk fibers in a wide range of spinning conditions. The mechanical behavior and microstructure of these high performance fibers have been characterized, and compared with those fibers produced through conventional spinning conditions. The comparison reveals that both sets of fibers share a common semicrystalline microstructure, but significant differences are apparent in the amorphous region. Besides, high performance fibers show a ground state and the possibility of tuning their tensile behavior. These properties are characteristic of spider silk and not of natural silkworm silk, despite both regenerated and natural silkworm silk share a common composition different from that of spider silk.

KEYWORDS: biofibers; biomimetic; silk

INTRODUCTION Biomimetics has emerged as the discipline that intends to expand and organize the knowledge required to regain the singular properties of biological materials and structures in artificial systems.[1] The development of the field has shown that this objective cannot be the result of simply learning how to copy the building blocks and mechanisms of natural processes. Instead, it is commonly accepted that it must be the result of gaining a deep understanding on the principles involved in the organization of the biological constituents and their interactions. However, the fulfilment of this basic program has revealed itself as extremely involved, not only due to the difficulties associated with the study of each individual level of organization and processing, but also due to their subtle interplay.

The production of artificial fibers inspired in natural silks represents a paradigmatic example of these difficulties. Natural silk fibers are the result of a balanced combination between carefully tailored compositions and highly sophisticated spinning glandular systems. The singularities of the proteins that form silk, known generically as fibroins,[2,3] include their large molecular weight,[3,4] the large amount of the small amino acids glycine and alanine[5] and, even more strikingly, the conservation of their main motifs and overall organization for a period of over 100 million years.[6] Besides, the formation of the solid fiber from the initial protein dope apparently involves the organization of the proteins in a liquid crystalline phase,[7,8] and probably a number of steps in which the pH and ionic concentration of the dope change along the gland.[9–13]

In this context, the synthesis of artificial bioinspired fibers must face a number of severe limitations that prevents the simplistic copy of the natural system. Thus, genetic engineering techniques only allow cloning proteins with a molecular weight that goes typically from one fifth to one third of that observed in natural fibroins.[14] This limitation requires establishing previous hypothesis on which parts of the natural protein are essential for their performance and how they should be organized,[15,16] to decide the sequence of bioinspired silk proteins. Complicated as this choice may be, the situation is even more involved with regard to the development of the artificial spinning process. Although there are some reports of microfluidic devices that allow the modification of the pH of the dope during spinning,[15,17] most processes are based on the wet-spinning technique,[18] which requires the formation of a spinnable dope that solidifies into a fiber in a coagulating bath.

The relative ease with which silkworm silk fibroin can be obtained in comparison with spider silk fibroins has

stimulated the development of artificial spinning systems to produce regenerated silkworm silk fibroin fibers. In addition, the study of regenerated fibers just leaves one basic unknown (processing), whereas the other (composition) is the same as in the natural material. The procedures for spinning regenerated fibers differ essentially in the composition of the initial dope and, to a lesser extent, in the composition of the coagulation bath. Thus, a number of dope compositions that yield spinnable solutions were reported, such as saturated ammonium sulfate solution,[19] concentrated orthophosphoric acid,[20] concentrated aqueous solution,[21,22] hexafluoro-2-propanol,[23,24] hexafluoroacetone hydrate,[25] formic acid,[26,27] ionic liquids,[28,29] and N-methyl morpholine oxide.[30]

However, the production of regenerated silkworm silk fibers has represented an extremely painstaking effort, as reflected by the poor tensile properties reported by most studies.[22,27,30,31] It was only after introducing subsequent changes in the basic wet-spinning process, especially related with the introduction of modified postspinning drawing processes, when the first reports of the production of high performance regenerated silkworm silk fibroin fibers with properties comparable with those of the natural material were found.[32–35]

The availability of high performance regenerated fibers allows gaining a deeper understanding on the essentials of the spinning process by simply correlating the microstructure and tensile behavior of the fibers with the processing conditions under which they are spun. Following this rationale, we present here a systematic study on regenerated fibers subjected to immersion post-spinning drawing (IPSD).[34] The microstructure and tensile properties of fibers spun under different conditions are characterized, so that the range of conditions that yield high performance fibers can be identified. Besides, under these processing conditions, the appearance of supercontraction[36,37] jointly with the existence of a ground state[37,38] is assessed.

EXPERIMENTAL PROCEDURES

Spinnable dopes of silkworm silk fibroin obtained from the cocoons were prepared as described in detail elsewhere.[30,34] Silk fibroin concentration was fixed to 17% (w/w) with respect to the solution. Regenerated silkworm silk fibers were spun from the dopes with a dry-jet wet-spinning line composed of an extrusion unit, a coagulation bath, a take-up spool, an immersion postspinning drawing bath, that consists of a bath of water in which the spun fiber is subjected to postspinning drawing, and finally a collecting spool as shown in Figure 1.[34] Silk fibroin solutions were extruded at 90°C and at fixed rate $V_0 = 4$ m/min through a 100-μm hole spinneret with 50 mm of air gap into a coagulation bath of methanol. The coagulated thread was further stretched in the immersion postspinning drawing bath and finally collected on the roller. Each batch was characterized by two processing parameters: the ratio of the take-up speed (V_1) to the extrusion speed (V_0) denoted as DR_1 ($DR_1 = V_1/V_0$), and the ratio of the roller speed (V_2) to the take-up speed (V_1) denoted as DR_2 ($DR_2 = V_2/V_1$) (see Fig. 1).

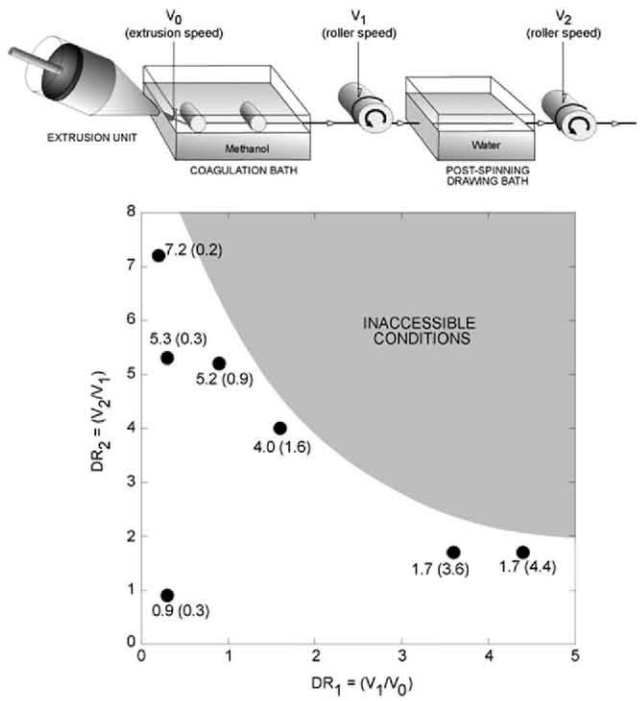

FIGURE 1 Postspinning drawing conditions of the samples presented in this work. DR_1 is defined as the ratio between take-up speed and extrusion speed ($DR_1 = V_1/V_0$) and DR_2 is defined as the ratio between postspinning drawing speed and take-up speed ($DR_2 = V_2/V_1$). The processing route is schematically shown, and the velocities that define the process are illustrated.

Two kinds of IPSD samples were considered: the as spun (AS) fibers, collected from the spinning line, and the maximum supercontracted (MS) samples, that were obtained from AS specimens through a supercontraction process. The supercontraction process proceeded as explained elsewhere[39]: AS samples were immersed in water for 24 h, allowed to contract freely and dried overnight. The percentage of supercontraction %SC is defined as $100 \times (L_0\text{-}L_{MS})/L_0$, where L_0 is the initial length of the AS fiber and L_{MS} its length after maximum supercontraction.

To measure the diameters of AS fibers, two small pieces (5-mm long) adjacent to both sides of each sample were retrieved, metallized with gold, and observed in a scanning electron microscope (SEM-JEOL 6300). The samples were observed at 10 kV and $I = 0.06$ nA. The cross-sectional area was computed assuming a circular cross-section and diameters at a given section of the fiber were calculated as the average of at least 10 measurements. MS cross-sectional areas were derived from AS ones under the hypothesis of volume constancy, a conventional assumption for the calculation of stresses in silks,[40] that was proven for major ampullate gland silk.[41] The constancy of volume after supercontraction in IPSD fibers was further validated by comparing the diameters of supercontracted fibers with those of adjacent fibers and by taking into account the reduction in length. True stresses were calculated under the hypothesis of volume constancy during the tensile test.

To measure the mechanical properties, samples from the different batches were mounted on perforated cardboard cards. Each sample was glued across a rectangular hole, to give a gauge length of 25 mm and tensile tested, as reported elsewhere.[42] An electronic balance (AND 1200G; resolution 0.1 mN) under the lower grip was used instead of a conventional load cell to measure force. The crosshead was moved with a constant and fixed rate equal to 2 mm/min and the measurements were performed at 25°C and 35% relative humidity. At least four samples from any given batch and condition (AS or MS) were tensile tested.

To determine microstructural parameters, synchrotron radiation microdiffraction experiments were performed at the ESRF-ID13 beamline using an $\approx 1 \times 1\ \mu m^2$ monochromatic beam from crossed mirrors at a wavelength of 0.09614 nm, as explained in detail elsewhere.[34,43] A minimum of 20 observations were made on each sample, X-ray diffraction (XRD) patterns of hydrated samples were obtained by using a closed humidity cell with mica windows. Humidity saturation conditions were defined at room temperature ($\approx$ 20°C) by observing excess of water condensed in the cell. XRD data were used to study the unit cell of the fibers, their crystallinity, the sizes of the nanocrystals, and their orientation with respect to the fiber's macroscopic axis.[44] Crystallinity was determined from $\chi = \Sigma I_B/(\Sigma I_B + I_{sr})$ where ΣI_B is the sum of intensities of Bragg peaks and I_{sr} is the short-range order background.[43] The particle size was determined by Scherrer's equation $L = (0.9\ \lambda)/(B\cos\Theta)$ where λ is the wavelength, B the radial width (fwhm) and Θ the Bragg angle.[45] L corresponds to a lower size limit for coherently scattering crystallites. Finally, the orientation of the nanocrystals was measured by the degree of orientation defined as $f_c = (3<\cos^2\phi_1>-1)/2$, where $<\cos^2\phi_1>$ is determined from the azimuthal broadening of the equatorial 210/100 reflections.[46]

The birefringence of IPSD fibers was measured using a polarizing microscope Reichert with crossed polars fitted with an Ehringhaus compensator. IPSD fibers were placed on a glass slide and the measurements were done in air. The angle of retardation was measured and converted to birefringence (Δn). The average birefringence values were the result of at least five measurements in different points along the fibers.

RESULTS AND DISCUSSION

Mechanical Behavior of AS IPSD Regenerated Silk Fibers

Figure 1 outlines the whole range of processing conditions analyzed in this work. Each batch is labeled by the pair $DR_2(DR_1)$, where DR_2 is the ratio of the postspinning drawing speed and the take-up speed, and DR_1 (number in parenthesis) is the ratio between the take-up speed and the extrusion speed. The choice in the format of the label is dictated, as it will be clear from the data presented below, by the importance of DR_2 in the behavior of the fibers. As it is also indicated in Figure 1, there is a range of inaccessible conditions at high postspinning drawing speeds due to the limitation in the maximum velocity that the fibers could withstand during spinning without breaking. As it is apparent from Figure 1, the batches studied in this work essentially cover the whole range of accessible processing conditions.

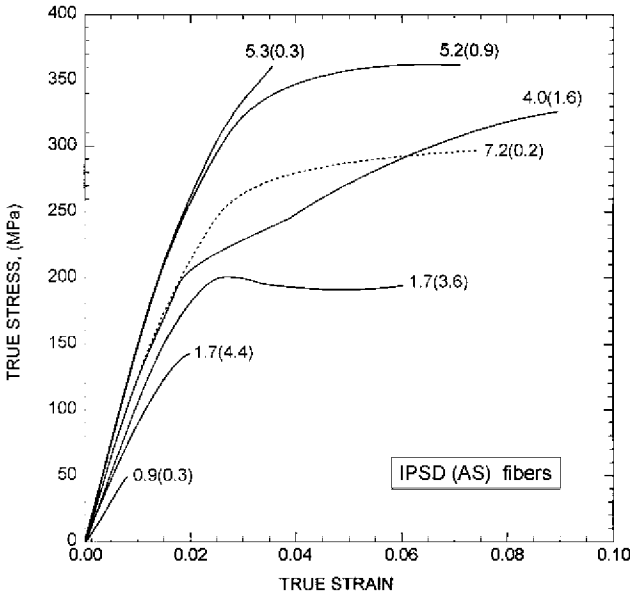

FIGURE 2 True stress versus true strain curves for IPSD fibers in the AS condition retrieved from the batches with different take-up speed (V_1) and postspinning drawing speed (V_2). Each curve is labeled by the pair $DR_2(DR_1)$ (see Fig. 1).

Representative true stress-true strain curves of samples in the AS condition retrieved from the batches produced with different postspinning drawing and take-up speeds are shown in Figure 2 and their main mechanical parameters are outlined in Table 1. A general tendency to significant increases in the elastic modulus and tensile strength with increasing postspinning drawing ratio, DR_2, is observed in Figure 2, although isolated deviations from this tendency are observed in the samples spun at low take-up speed [batch 7.2(0.2)]. Strain at breaking shows a less identifiable trend, probably indicating that both DR1 and DR2 influence the value of this mechanical parameter. In contrast, the diameter of fibers seems to be especially sensitive to the take-up speed, V_1, as indicated by the increase diameter of fibers spun at low DR_1 ratios (low V_1). This correlation, however, is not perfect, indicating that the postspinning drawing ratio, DR2, must exert some influence on this geometrical parameter. As it had been reported in previous works,[31] fibers spun at low postspinning drawing speeds show a brittle behavior with a very low strain at breaking, and ductility tends to increase in samples spun at higher postspinning drawing ratios.

Contraction and Tensile behavior in Water

Although the tensile properties shown in Figure 2 are remarkable for regenerated fibers, probably the most striking feature of IPSD fibers is the existence of a supercontraction effect as reported previously,[34] and described in detail below. Supercontraction was first identified in the silk spun from the major ampullate gland of spiders as a significant reduction in the length of the fiber when immersed unrestrained in water.[36] The tensile properties of supercontracted fibers

TABLE 1 Diameter and Mechanical Parameters of the Immersed Post Spinning Drawn (IPSD) Samples Tested in the As Spun (AS) Condition

Spinning Conditions $DR_2(DR_1)$	D(μm)	E (GPa)	σ_u (MPa)	ε_u	W_f (MJ/m^3)
0.9(0.3)	55 ± 2	6.6 ± 0.4	46 ± 7	0.0075 ± 0.0005	0.16 ± 0.04
1.7(4.4)	13.4 ± 0.5	9.1 ± 0.3	127 ± 5	0.03 ± 0.01	3 ± 1
1.7(3.6)	19 ± 1	10.0 ± 0.3	200 ± 2	0.06 ± 0.02	10 ± 2
4.0(1.6)	13.3 ± 0.5	13.4 ± 0.3	325 ± 2	0.09 ± 0.01	20 ± 3
5.2(0.9)	18.4 ± 0.4	14.2 ±0.3	351 ± 9	0.07 ± 0.01	18 ± 4
5.3(0.3)	32 ± 2	13.7 ± 0.3	360 ± 10	0.039 ± 0.001	8.7 ± 0.6
7.2(0.2)	41 ± 4	12.2 ± 0.3	320 ± 20	0.056 ± 0.007	12 ± 2

E, elastic modulus; σ_u, tensile strength; ε_u, strain at breaking; W_f, work to fracture measured as the area under the stress-strain curve.

The first number of the spinning conditions indicates the post-spinning drawing ratio, DR_2, and the number in parenthesis indicates the take-up ratio, DR_1.

tested in water were found to correspond to that of an elastomer,[47] characterized by a very low initial elastic modulus and an increase in stiffness with increasing deformation. It was later acknowledged that supercontraction was the most evident mark of a characteristic property of spider silk: the existence of ground state[37] to which the fiber can revert through a supercontraction process independently from its previous loading history.[38,39] This finding has suggested a redefinition of the concept supercontraction,[48] which is now defined by the existence of a ground state, and not by a contraction in water beyond a given limit, since some silk fibers contract when immersed in water but do not recover.

Samples from all of the studied batches (no data were obtained for the batch 0.9(0.3), since all fibers broke during the supercontraction process) were observed to reduce their length upon immersion in water down to ~12% of its initial length [mimimum value 11% for batch 1.7(4.4), maximum value 14% for batch 7.2(0.2)]. The reduction in length was observed to increase further upon drying as shown by the values of the total percentage of supercontraction presented in Table 2.

TABLE 2 Percentage of Total Contraction of the Regenerated Samples

Spinning Conditions $DR_2(DR_1)$	% SC
1.7(4.4)	21 ± 2
1.7(3.6)	24 ± 4
4.0(1.6)	21 ± 1
5.2(0.9)	20 ± 4
5.3(0.3)	22 ± 3
7.2(0.2)	24 ± 1

The first number of the spinning conditions indicates the post-spinning drawing ratio, DR_2, and the number in parenthesis indicates the take-up ratio, DR_1.
The percentage of supercontraction %SC is defined as $100\times(L_0\text{-}L_{MS})/L_0$, where L_0 is the initial length of the fiber and L_{MS} its length after maximum supercontraction.

The true stress-true strain curves of IPSD fibers when immersed in water are shown in Figure 3(a). It seems that the strain at breaking decreases and the tensile strength increases with increasing postspinning drawing ratio, DR_2, up to $DR_2 = 5.2$. It is also apparent that for postspinning drawing ratios equal or higher to 4.0 only small differences are exhibited by the fibers in terms of their tensile properties in water. Figure 3(b) shows tests performed in air and in water to allow an easier comparison of the behavior of IPSD fibers under both conditions.

Tensile Properties of MS Fibers

As indicated above, contraction in water by itself does not necessarily imply the existence of a ground state.[49,50] To assess the existence of a ground state it is possible to check a number of properties, one of the most evident being the significant change in the tensile properties of supercontracted fibers compared with those observed in the AS condition. Figure 4(a) shows representative true stress-true strain curves of the samples in the MS condition. No results are shown for the condition 0.9(0.3) because the brittleness of these fibers led to its breaking before the supercontraction process could be completed. Comparison with the behavior of the fibers in the AS condition presented in Figure 2 shows that immersion in water leads to significant changes in the properties of the fiber, as shown in Figure 4(b).

The percentage of total contraction, that is, contraction after immersion and subsequent drying, is indicated in Table 2. As it was mentioned above, contraction proceeds in two steps: an initial contraction in water and an additional contraction after overnight drying. The dimensional variation between wet and dried fibers was previously found in regenerated fibers,[50] and explained by the swelling that results from the penetration of water molecules in the structure of the fiber. The total percentage of supercontraction (%SC) exhibited by the fibers is close to %SC ≈22% for all batches.

From the results presented in Figure 4, it is apparent that the tensile properties of the MS samples can be grouped into two regimes related with the processing conditions. The mechanical behavior exhibited by the batch 1.7(4.4) indicates

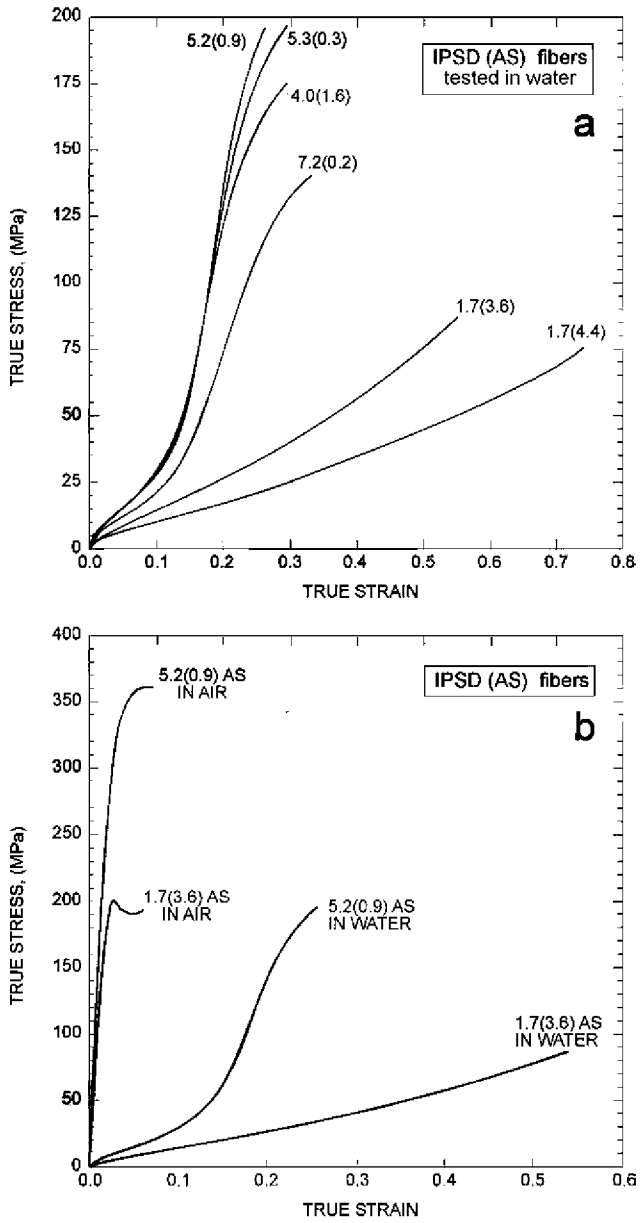

FIGURE 3 (a) True stress versus true strain curves for IPSD fibers from the different batches tested in water. (b) Comparison of selected true stress-true strain curves of IPSD fibers either tested in water or in air (AS condition). Each curve is labeled by the pair $DR_2(DR_1)$.

that, at given combinations of low postspinning drawing ratio and take-up speed, the immersion step does not exert significant influence on the tensile properties. Samples that belong to this group do not show appreciable differences between the AS and the MS conditions.

The other regime is exhibited by batches with high postspinning drawing ratios, which show an increase in the strain at breaking and a region at large deformations where the slope of the stress–strain curve increases with strain. Although there are slight differences in the values of the tensile strength and strain at breaking of the different batches that belong to the second regime, their combination yields a work to fracture of $W_f \approx 54$ MJ/m^3 in all cases. This is a significantly high value that compares well with that reported for natural *Bombyx mori* silk fibers $W_f \approx 50$–60 MJ/m.[3,51,52]

Batch 1.7(3.6) illustrates the limit between both regimes. The limiting behavior is characterized by the increase in the strain at breaking of samples in the MS condition, but the tensile strength is similar to the yield stress (i.e., the stress at the end of the initial linear region of the curve), so that no increase in the slope of the stress–strain curve at large deformations is observed. The limiting character of the batch

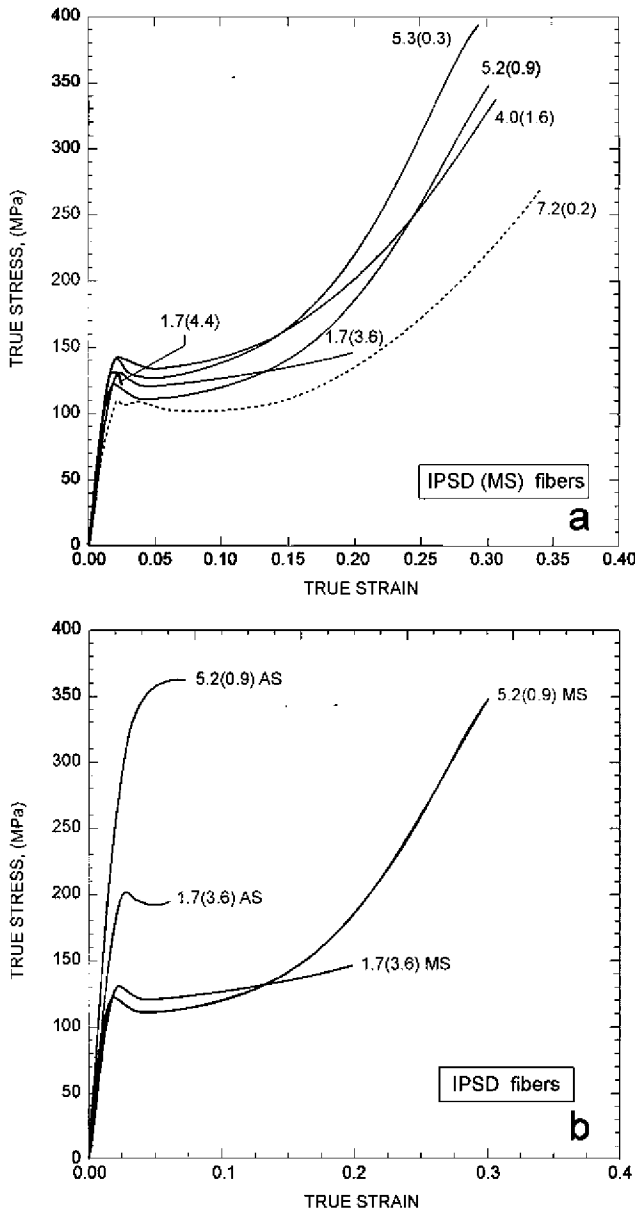

FIGURE 4 (a) True stress versus true strain curves for IPSD fibers in the MS condition from the different batches. (b) Comparison of selected true stress-true strain curves of IPSD fibers either in the MS condition or in the AS condition. Each curve is labeled by the pair $DR_2(DR_1)$.

TABLE 3 Mechanical Parameters of the Regenerated Samples Tested in the Maximum Supercontracted (MS) Condition

Spinning Conditions $DR_2(DR_1)$	σ_u (MPa)	ε_u	W_f (MJ/m^3)
1.7(4.4)	120 ± 20	0.02 ± 0.01	2.1 ± 0. 9
1.7(3.6)	160 ±20	0.2 ±0.1	27 ± 10
4.0(1.6)	340 ±10	0.30 ±0.01	58 ± 3
5.2(0.9)	380 ± 10	0.29 ±0.01	56 ± 3
5.3(0.3)	340 ± 20	0.29 ±0.01	50 ± 4
7.2(0.2)	273 ± 6	0.34 ± 0.01	52 ± 2

σ_u, tensile strength; ε_u, strain at breaking; W_f: work to fracture, measured as the area under the stress-strain curve.
The first number of the spinning conditions indicates the post-spinning drawing ratio, DR_2, and the number in parenthesis indicates the take-up ratio, DR_1.

1.7(3.6) and its close dependence on the detailed processing conditions is highlighted by the large standard deviations in the strain at breaking observed in the samples of this batch both in the AS and in the MS condition as indicated in Tables 1, 2, and 3.

Existence of a Ground State

As previously mentioned, the essential feature of a ground state is the possibility that the fiber can always revert to this state independently from the loading history of the sample. Besides, the mechanical properties of fibers with a ground state can be accurately tailored with a simple process.[38] The ground state is reached after subjecting the fiber to a maximum supercontraction process, and represents the most compliant condition of the material.[37] Figure 5 shows recovery tests[39] on samples from two different batches: 4.0(1.6) and 1.7(3.6). Recovery tests proceeded by stretching in air up to a predetermined length fibers in the MS condition. After stretching, the fiber was subjected to a new supercontraction step and tensile tested after drying. If the curves obtained from both processes concur, the fiber was said to recover from otherwise irreversible deformation. Figure 5 shows that samples from both batches recover and, consequently, present a ground state. Following previous discussions,[34] the existence of a ground state to which the fiber can revert distinguishes genuine supercontraction from the simple contraction in water.

An outstanding consequence of the existence of a ground state is that the properties of the material can be modified in a predictable and reproducible way. Thus, it has been found that the wide range of tensile properties exhibited by spider silk fibers[53] can be replicated at will by simply stretching in water fibers in the MS condition up to the chosen length and drying subsequently, in a process known as wet stretching.[38] MS condition simply corresponds to the limiting case in which the fiber is not stretched. Figure 6 presents the true stress-true strain curves of samples from the batch 5.3(0.3) subjected to different wet stretching processes. Each process was characterized by its alignment parameter, α, defined as $\alpha = L_C/L_{MS}$-1, where L_{MS} is the length

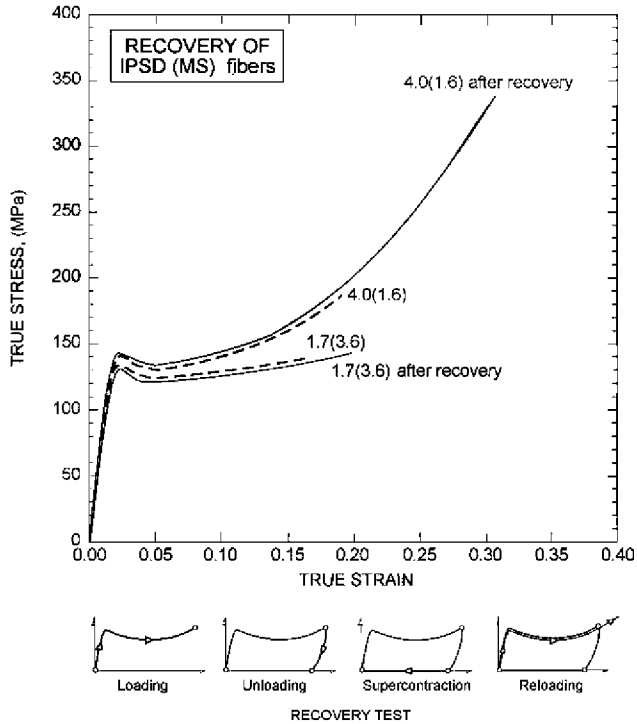

FIGURE 5 Recovery tests on fibers from two different batches. The recovery test consists of stretching a supercontracted fiber up to a given strain (in this case $\varepsilon \approx 0.2$) and subjecting the fiber to a new maximum supercontraction step. The stress–strain curve of the supercontracted fiber and that measured after stretching and subsequent supercontraction concur, which indicates the existence of a ground state in the fibers of both batches.

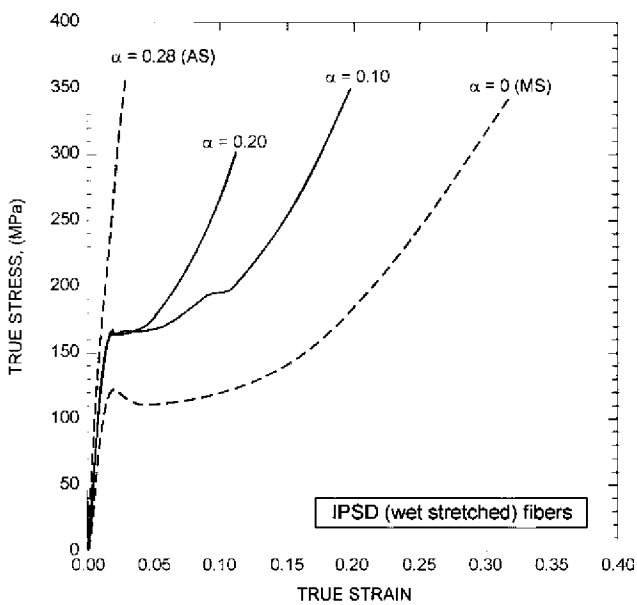

FIGURE 6 True stress versus true strain curves for IPSD fibers of the batch 5.3(0.3) with different values of the alignment parameter, α. By definition the lowest level of the alignment parameter, $\alpha = 0$, corresponds to the MS condition. The highest value of α corresponds to the AS condition.

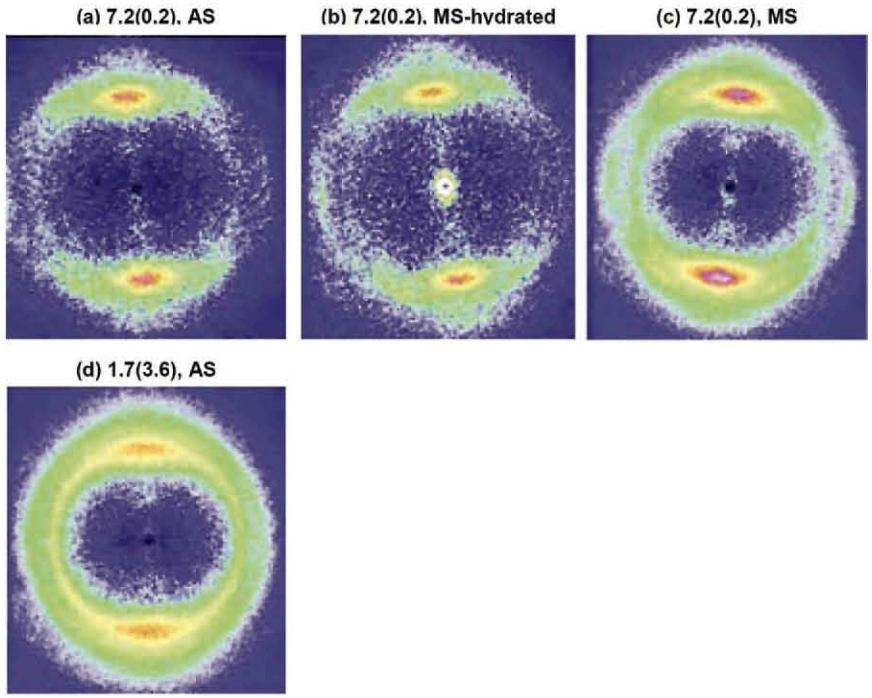

FIGURE 7 X- ray diffraction diagrams of regenerated silk fibers of the 7.2(0.2) batch in the (a) AS condition, (b) MS-hydrated condition and (c) MS condition, and (d) of the 1.7(3.6) batch in the AS condition. The macroscopic axis of the fiber is oriented approximately along the horizontal direction.

of the fiber after maximum supercontraction and L_C is the length of the fiber after wet stretching. α ranges from $\alpha = 0$ (MS condition) to $\alpha = 0.28$ (AS condition). It is evident that the strain at breaking and the compliance of the samples decreases monotonically with increasing values of the parameter of alignment.

Microstructural Analysis

The XRD patterns of IPSD regenerated fibers of the batch 7.2(0.2) in the AS, MS—dry condition—(MS), MS in a water saturated environment (MS-hydrated), and of the batch 1.7(3.6) in the AS condition are shown in Figure 7, and their main microstructural parameters are presented in Table 4. The microstructural patterns obtained from the XRD patterns are presented in Table 1. All regenerated fibers show the same reflections that can be indexed for the same orthorhombic unit cell as *Bombyx mori* silk fibers.[54] The orientation of the equatorial 210-reflection indicates that the protein backbone is oriented along the macroscopic fiber axis.

The crystallinity of the batch 7.2(0.2) in the AS condition was estimated as 20% and remained practically unchanged in both the MS and MS-hydrated conditions. Despite differences in the processing conditions, the crystallinity of the batch 1.7(3.6) yields a very similar value of 22%. These values of crystallinity are comparable with those reported for spider silk (crystallinity $\approx$ 10–15%)[55] and considerably smaller than those found in natural *Bombyx mori* silk fibers, 56–65 %.[7,43]

From the radial profile of the 010/210-reflections, particle sizes in the nm-range were obtained (Batch 7.2(0.2): AS: 3.0 nm, MS: 2.7 nm, MS-hydrated: 2.8 nm; Batch 1.7(3.6): AS: 2.4 nm). These dimensions are similar to nanodomains observed for natural *Bombyx mori*,[43] although a significantly larger dimension along the hydrogen-bonded [210]-direction as for natural *Bombyx mori* silk is not observed.

TABLE 4 Comparison of the Microstructural Parameters of the AS- and MS-Fibers, as Obtained by X-ray Diffraction

Sample	f_c	*L* [210] Particle Size (nm)	*L* [200] Particle Size (nm)	X × 100 Crystallinity (%)
AS 7.2(0.2)	0.85	3.0	~2	20
MS 7.2(0.2)	0.79	2.7	~3	20
MS-hydrated 7.2(0.2)	0.84	2.8	~2	22
AS 1.7(3.6)	0.81	2.4	2.5	22

The 200-reflection is located in the lower-Q tail of the 210-reflection and the determination of peak broadening and hence particle size is less precise.

TABLE 5 Birefringence Values of Samples from Different Batches in the AS and MS Conditions

Spinning Conditions $DR_2(DR_1)$	AS Δn	MS Δn
1.7(4.4)	0.022 ± 0.003	0.019 ± 0.002
1.7(3.6)	0.027 ± 0.003	0.024 ±0.004
4.0(1.6)	0.037 ± 0.001	0.035 ±0.002
5.2(0.9)	0.037 ± 0.002	0.035 ± 0.003
5.3(0.3)	0.042 ± 0.004	0.037 ± 0.005
7.2(0.2)	0.042 ± 0.005	0.037 ± 0.004

The first number of the spinning conditions indicates the post-spinning drawing ratio, DR_2, and the number in brackets indicates the take up ratio, DR_1.

The degree of orientation, f_c, was determined from the analysis of the azimuthal intensity profile of the 210-reflection.[44] The results show that the degree of orientation is similar for all the conditions. The values of the degree of orientation are comparable with that reported for the major ampullate gland silk of *Nephila* spiders,[56,57] and significantly lower than that measured for *Bombyx mori* samples under similar experimental conditions.[43]

The comparison of the degrees of orientation of the samples AS, MS, and MS-hydrated of the batch 7.2(0.2) indicated that the nanodomains slightly lose their alignment along the fiber axis during supercontraction. A similar loss of alignment was described for supercontracted spider silk fibers.[58] It is also found that the degree of orientation of the MS-hydrated fiber is larger than that of the MS–dry condition–sample.

The microstructural analysis of the samples was completed with birefringence data. Birrefringence conveys information on the anisotropy of the samples, although it does not allow discriminating between the orientation of chains in the crystalline and amorphous fractions. The results of the birefringence measurements on AS and MS conditions, presented in Table 5, indicate that the overall alignment of the protein chains decreases in the MS conditions, in agreement with the loss of alignment of the nanodomains observed in XRD data.

Besides, a tight correlation can be established clearly between birefringence and tensile properties in the MS condition. Thus, samples of the batch 1.7(4.4), characterized by a small strain at breaking and tensile strength, show the lowest value of birefringence ($\Delta n = 0.019$). In contrast, all batches spun at postspinning drawing speed larger than 4.0, characterized by large strain at breaking and tensile strength, show comparable values of birefringence ($\Delta n \approx 0.036$). The batch 1.7(3.6) shows an intermediate value of birefringence in correspondence with its intermediate tensile behavior characterized by a relatively large strain at breaking, but a low increase in its tensile strength.

FINAL COMMENTS AND CONCLUSIONS

The present data demonstrate that immersion postspinning drawing (IPSD) yields high performance regenerated fibers under a wide range of processing speeds. Besides, it is shown that immersion postspinning drawing is a critical step in this process, as fibers postspinning drawn in air or, even if immersed in water, not sufficiently stretched (i.e., fibers spun at low values of DR_2) only show marginal improvements, if any, in their mechanical behavior (see Fig. 2).

Consequently, identifying the effect that immersion postspinning drawing exerts on initially very brittle fibers, turning them into tough fibers endowed with additional properties appears as the critical point of this work. In this regard, Figure 8 compares the tensile behavior and the basic microstructural features of samples subjected to the different postspinning steps, and is intended to help in the following discussion.

Regenerated brittle fibers are obtained if no postspinning drawing is applied. The analysis by atomic force microscopy showed that brittle samples present a homogeneous microstructure characterized by nanoglobules, which are smaller than those found in natural silkworm silk fibers.

The introduction of a postspinning drawing step in air led to an increase in ductility in the fibers, as illustrated in Figure 8. Besides, the microstructural analysis by AFM[59] revealed that the ductile fibers showed a heterogeneous microstructure composed of two phases, in contrast to the homogeneous organization observed in brittle regenerated fibers[59] and in natural silk fibers.[60] In addition, one of the phases was comparable in terms of the size of the nanoglobules with that observed in brittle fibers. The emergence of a second phase with smaller microstructural details was consistent with a new organization of the fibroin proteins induced by the postspinning drawing step. The presence of large areas

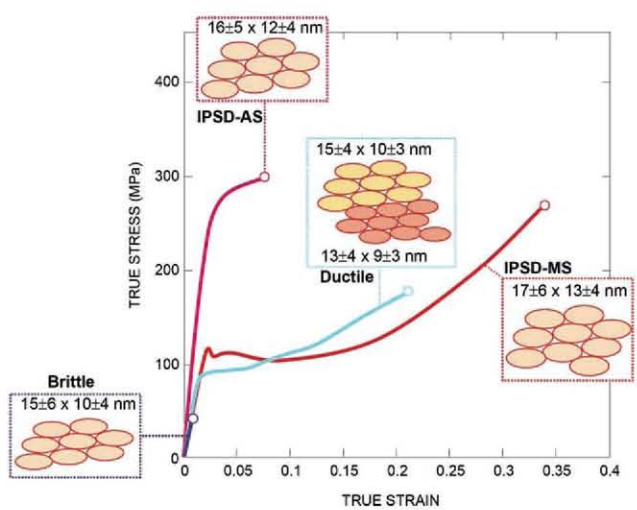

FIGURE 8 Comparison of the tensile behavior and microstructure, as observed with atomic force microscopy, of the regenerated fibers not subjected to postspinning drawing in air (brittle), subjected to a postspinning drawing in air (ductile), immersion postspinning drawn fibers in the as spun condition (IPSD-AS), and immersion postspinning drawn fibers after maximum supercontraction (IPSD-MS).

with the original microstructure (i.e., that observed in brittle samples) suggested that the transition between both microstructures was not completed during the postspinning drawing step in air.

In contrast, the microstructure of IPSD fibers appears homogeneous when observed by AFM[34] both in the AS and MS conditions, indicating that the incipient transformation during postspinning drawing in air is completed if the postspinning proceeds with the fiber immersed in water.

To identify the mechanism responsible for the microstructural changes induced by postspinning drawing, it is very revealing to compare the tensile behavior in water of the different sets of fibers tested. Brittle fibers showed a very different mechanical behavior when tested in water,[50] characterized by a large increase in ductility and a large drop in their tensile strength. In contrast, fibers subjected to a postspinning drawing step in air showed a large drop in their tensile strength, but no significant variation in their strain at breaking. It was further found that brittle fibers could reach the properties of the ductile fibers (i.e., spun with a postspinning drawing step) by simply stretching while immersed in water.[50] This way the tensile characterization in water revealed a close connection between both sets of fibers.

At this stage, it was proposed that the tensile behavior of regenerated fibers could be explained as the result of the combination of hydrogen bonding and a large number of entanglements,[61,62] absent in natural silkworm silk. Under this assumption, brittle samples (i.e., spun without postspinning drawing) would present an extremely large number of entanglements which, in combination with strong hydrogen bonding, would prevent conformational changes of the protein chains under external loading. This hypothesis is consistent with the accepted models of the mechanical behavior of silk that predict the existence of an initial elastic regime, in which the hydrogen bonds between chains in the amorphous matrix are sequentially broken,[62] followed by the unfolding of the secondary structures[63] and the increase in the load supported by the nanocrystals.[64] These two latter mechanisms are supposed to be responsible for the large strain at breaking reached by natural silks.

In this context, the behavior of brittle regenerated samples would be the result of the quick building up of stresses in largely immobilised chains. Since the chains are not free to unfold from the conformation reached during processing, the breaking of the material would occur at low strains. When the brittle fibers are immersed in water, hydrogen bonds would collapse and the chains would be allowed to sustain conformational changes without reaching large stresses. This model is compatible with the increase in the strain at breaking and with the decrease of the tensile strength observed in brittle fibers tested in water. Under this hypothesis ductility in fibers subjected to postspinning drawing would be related to an improved organization of the protein chains, that allows larger conformational changes in the proteins. However, the microstructural analysis by AFM shows that this improved organization can only be reached in some regions of the fiber, while the others would keep their initial organization. Thus, it is natural to argue that the role of water during the immersion postspinning drawing step is to increase the mobility of the protein chains during processing, so that this improved organization extends throughout the fiber. A similar mechanism has been proposed to explain the increase in tensile strength and strain at breaking in fibroin films subjected to uniaxial stretching.[65] In this case, it was hypothesized that the increased extensibility of regenerated silk fibroin films was the result of the disentangling of fibroin chains during the stretching step.

The microstructural data presented above from birefringence and XRD data render significant support to this hypothesis, as it was found that high performance is associated with an improved alignment of the fibers along the macroscopic axis of the fiber. Besides, this improved alignment can be assigned to the amorphous matrix, as the basic features of the nanocrystals remain essentially unchanged in the range of processing conditions explored. Consequently, the crystalline and amorphous fractions of the fiber seem to be affected by different processing parameters. The independence of the parameters that define the crystalline fraction from postspinning processing indicates that the crystalline fraction is most likely[66] fixed in the initial steps of fiber formation. Consequently, it is likely to assume that modifying the crystalline fraction of the fibers would require major changes in the composition of the dope and in the flow conditions during spinning. In this regard, it is of critical importance that the wet-spinning process allows reaching adequate values of the crystalline parameters, as it has been found that the size of the nanocrystals[67] is essential for the optimum tensile behavior of silk fibers. The crystalline fraction is not observed to undergo variations during supercontraction or stretching as shown in Table 4, so that these processes only cause the rotation of the nanocrystals. Spider silk is thought to exhibit a similar behavior since nanocrystals can rotate, but the crystalline fraction does not seem to be altered.[68]

Consequently, the evolution of the mechanical properties from brittle to high performance fibers is consistent with microstructural changes that occur in the amorphous regions, in particular an increase in the mobility of the protein chains. In this regard, the increase in the strain at breaking in the intermediate 1.7(3.6) batch is compatible with the initial regime of an elastomeric behavior, in which large strains are reached at low forces. This result is also supported by the mechanical behavior of the brittle fibers in water which shows that upon collapse of interchain hydrogen bonds, silk proteins are able to sustain considerable stretching, but under very low loads. In contrast, high performace fibers show a monotonic increase of stress with strain at large deformations, which is responsible for the high work to fracture reached by these fibers [see Fig. 4(b)]. This behavior is compatible with the increase in stiffness characteristic of elastomeric polymers that can reach a regime of moderate to large strains.

In conclusion, the analysis of regenerated silk fibers casts light on several aspects of the processing route and on its relationship to the microstructure and properties of the fibers, which can be outlined as follows:

1. Immersion postspinning drawing (IPSD) provides a reliable processing route for the production of high performance regenerated fibers under a variety of experimental conditions in terms of take-up and postspinning drawing speeds.
2. Values of the work of fracture measured from IPSD fibers in the MS condition spun under a wide range of processing conditions are comparable with those of natural *Bombyx mori* silk, showing the reliability of the technique. However, the detailed behavior of IPSD differs from that of natural silkworm silk, since tensile strength is lower and strain at breaking is higher compared with the natural material.
3. High performance in IPSD fibers is associated with an improved organization of the protein chains, reflected by an increased alignment of the chains along the macroscopic axis of the fiber.
4. All IPSD fibers contract in water, but only in high performance fibers spun at sufficient postspinning drawing speeds this effect is associated with the existence of a ground state, that is, a state to which the fiber can revert independently from the previous loading history. The crystalline fraction does not vary during contraction, but nanocrystals rotate to an extent that correlates with the percentage of supercontraction.
5. All the results are consistent with the assumption that the high mobility of the protein chains during immersion in water, combined with the stresses generated during postspinning drawing yield an improved arrangement of the chains and a reduction in the density of entanglements in the amorphous region. In contrast to regenerated fibers subjected to postspinning drawing in air, immersion in water allows this process to be completed homogeneously within the fiber.

ACKNOWLEDGMENTS

The authors would like to thank Mario Traverso for his helpful work on the wet-spinning line and Dr. G. Freddi (Stazione Sperimentale per la Seta, Milan, Italy) for providing silkworm silk fibroin. The authors are grateful to José Miguel Martínez for his help with the artwork. The work was funded by Ministerio de Educación y Ciencia (Spain) through project MAT 2009-10258, by the Comunidad de Madrid (Spain) (Grant CCG10-UPM/MAT-5698) and by Fundación Marcelino Botín.

REFERENCES

1 Schmitt, O. H. In Some Interesting and Useful Biomimetic Transforms; Proceedings of Third International Biophysics Congress; Massachusetts **1969**, p 297.

2 Xu, M.; Lewis, R. V. *Proc. Natl. Acad. Sci. U. S. A.* **1990,** *18,* 7120–7124.

3 Xia, Q. Y.; Zhou, Z. Y.; Lu, C.; Cheng, D. J.; Dai, F. Y.; Li, B.; Zhao, P.; Zha, X. F.; Cheng, T. C.; Chai, C. L.; Pan, G. Q.; Xu, J. S.; Liu, C.; Lin, Y.; Qian, J. F.; Hou, Y.; Wu, Z. L.; Li, G. R.; Pan, M. H.; Li, C. F.; Shen, Y. H.; Lan, X. Q.; Yuan, L. W.; Li, T.; Xu, H. F.; Yang, G. W.; Wan, Y. J.; Zhu, Y.; Yu, M. D.; Shen, W. D.; Wu, D. Y.; Xiang, Z. H.; Yu, J.; Wang, J.; Li, R. Q.; Shi, J. P.; Li, H.; Li, G. Y.; Su, J. N.; Wang, X. L.; Li, G. Q.; Zhang, Z. J.; Wu, Q. F.; Li, J.; Zhang, Q. P.; Wei, N.; Xu, J. Z.; Sun, H. B.; Dong, L.; Liu, D. Y.; Zhao, S. L.; Zhao, X. L.; Meng, Q. S.; Lan, F. D.; Huang, X. G.; Li, Y. Z.; Fang, L.; Li, C. F.; Li, D. W.; Sun, Y. Q.; Zhang, Z. P.; Yang, Z.; Huang, Y. Q.; Xi, Y.; Qi, Q. H.; He, D. D.; Huang, H. Y.; Zhang, X. W.; Wang, Z. Q.; Li, W. J.; Cao, Y. Z.; Yu, Y. P.; Yu, H.; Li, J. H.; Ye, J. H.; Chen, H.; Zhou, Y.; Liu, B.; Wang, J.; Ye, J.; Ji, H.; Li, S. T.; Ni, P. X.; Zhang, J. G.; Zhang, Y.; Zheng, H. K.; Mao, B. Y.; Wang, W.; Ye, C.; Li, S. G.; Wang, J.; Wong, G. K. S.; Yang, H. M. *Science* **2004,** *5703,* 1937–1940.

4 Ayoub, N. A.; Garb, J. E.; Tinghitella, R. M.; Collin, M. A.; Hayashi, C. Y. *PLoS ONE* **2007,** *6,* e514.

5 Lucas, F.; Shaw, J. T. B.; Smith, S. G. J. *Textile Inst.* **1955,** *46,* 440–452.

6 Gatesy, J.; Hayashi, C.; Motriuk, D.; Woods, J.; Lewis, R. *Science* **2001,** *291,* 2603–2605.

7 Kerkam, K.; Viney, C.; Kaplan, D.; Lombardi, S. *Nature* **1991,** *349,* 596–598.

8 Vollrath, F.; Knight, D. P. *Nature* **2001,** *410,* 541–548.

9 Jin, H. J.; Kaplan, D. L. *Nature* **2003,** *424,* 1057–1061.

10 Chen, X.; Shao, Z. Z.; Vollrath, F. *Soft Matter* **2006,** *6,* 448–451.

11 Heim, M.; Keerl, D.; Scheibel, T. *Angew. Chem. Int. Ed Engl.* **2009,** *20,* 3584–3596.

12 Askarieh, G.; Hedhammar, M.; Nordling, K.; Saenz, A.; Casals, C.; Rising, A.; Johansson, J.; Knight, S. D. *Nature* **2010,** *465,* 236–239.

13 Hagn, F.; Eisoldt, L.; Hardy, J. G.; Vendrely, C.; Coles, M.; Scheibel, T.; Kessler, H. *Nature* **2010,** *465,* 239–242.

14 Lazaris, A.; Arcidiacono, S.; Huang, Y.; Zhou, J. F.; Duguay, F.; Chretien, N.; Welsh, E. A.; Soares, J. W.; Karatzas, C. N. *Science* **2002,** *295,* 472–476.

15 Hardy, J. G.; Romer, L. M.; Scheibel, T. R. *Polymer* **2008,** *20,* 4309–4327.

16 Huemmerich, D.; Scheibel, T.; Vollrath, F.; Cohen, S.; Gat, U.; Ittah, S. *Current Biology* **2004,** *22,* 2070–2074.

17 Rammensee, S.; Slotta, U.; Scheibel, T.; Bausch, A. R. *Proc. Natl. Acad. Sci. U. S. A.* **2008,** *18,* 6590–6595.

18 Chawla, K. K. Fibrous Materials; Cambridge University Press: Cambridge, U.K., **1998.**

19 Yazawa, S. *J. Chem. Soc. Jpn* **1960,** *63,* 1428–1430.

20 Ishizaka, H.; Watanabe, Y.; Ishida, K.; Fukumoto, O. *J. Ser. Sci. Japan* **1989,** *58,* 87–95.

21 Matsumoto, K.; Uejima, H.; Iwasaki, T.; Sano, Y.; Sumino, H. *J Appl Polym Sci* **1996,** *4,* 503–511.

22 Xie, F.; Zhang, H. H.; Shao, H. L.; Hu, X. C. *Int. J. Biol. Macromol.* **2006,** *3–5,* 284–288.

23 Liivak, O.; Blye, A.; Shah, N.; Jelinski, L. W. *Macromolecules* **1998,** *9,* 2947–2951.

24 Trabbic, K. A.; Yager, P. *Macromolecules* **1998,** *2,* 462–471.

25 Yao, J. M.; Masuda, H.; Zhao, C. H.; Asakura, T. *Macromolecules* **2002,** *1,* 6–9.

26 Ha, S. W.; Tonelli, A. E.; Hudson, S. M. *Biomacromolecules* **2005,** *3,* 1722–1731.

27 Um, I. C.; Ki, C. S.; Kweon, H. Y.; Lee, K. G.; Ihm, D. W.; Park, Y. H. *Int. J. Biol. Macromol.* **2004,** *1–2*, 107–119.

28 Phillips, D.; Drummy, L.; Conrady, D.; Fox, D.; Naik, R.; Stone, M.; Trulove, P.; De Long, H.; Mantz, R. *J. Am. Chem. Soc.* **2004,** *44*, 14350–14351.

29 Phillips, D.; Drummy, L.; Naik, R.; De Long, H.; Fox, D.; Trulove, P.; Mantz, R. *J. Mater. Chem.* **2005,** *39*, 4206–4208.

30 Marsano, E.; Corsini, P.; Arosio, C.; Boschi, A.; Mormino, M.; Freddi, G. *Int. J. Biol. Macromol.* **2005,** *4*, 179–188.

31 Corsini, P.; Perez-Rigueiro, J.; Guinea, G. V.; Plaza, G. R.; Elices, M.; Marsano, E.; Carnasciali, M. M.; Freddi, G. *J. Polym. Sci. Part B: Polym. Phys.* **2007,** 2568–2579.

32 Corsini, P. New Fibres Based on Natural Polymers: Silk and Cellulose, Ph D Thesis; Universita degli Studi di Genova: Genova, **2008.**

33 Zhu, Z. H.; Ohgo, K. S.; Watanabe, R.; Takezawa, T.; Asakura, T. S. *J. Appl. Polym. Sci.* **2008,** *5*, 2956–2963.

34 Plaza, G. R.; Corsini, P.; Marsano, E.; Perez-Rigueiro, J.; Biancotto, L.; Elices, M.; Riekel, C.; Agullo-Rueda, F.; Gallardo, E.; Calleja, J. M.; Guinea, G. V. *Macromolecules* **2009,** *22*, 8977–8982.

35 Yan, J. P.; Zhou, G. Q.; Knight, D. P.; Shao, Z. Z.; Chen, X. *Biomacromolecules* **2010,** *1*, 1–5.

36 Work, R. W. *Text. Res. J.* **1977,** *10*, 650–662.

37 Perez-Rigueiro, J.; Elices, M.; Guinea, G. V. *Polymer* **2003,** *13*, 3733–3736.

38 Guinea, G. V.; Elices, M.; Perez-Rigueiro, J.; Plaza, G. R. *J. Exp. Biol.* **2005,** *1*, 25–30.

39 Elices, M.; Perez-Rigueiro, J.; Plaza, G.; Guinea, G. V. *J. Appl. Polym. Sci.* **2004,** *6*, 3537–3541.

40 Griffiths, J.; Salanitri, V. *J. Mater. Sci.* **1980,** *2*, 491.

41 Guinea, G. V.; Perez-Rigueiro, J.; Plaza, G. R.; Elices, M. *Biomacromolecules* **2006,** *7*, 2173–2177.

42 Perez-Rigueiro, J.; Viney, C.; Llorca, J.; Elices, M. *J. Appl. Polym. Sci.* **1998,** *12*, 2439–2447.

43 Martel, A.; Burghammer, M.; Davies, R. J.; Riekel, C. *Biomacromolecules* **2007,** *8*, 3548–3556.

44 Riekel, C.; Branden, C.; Craig, C.; Ferrero, C.; Heidelbach, F.; Muller, M. *Int. J. Biol. Macromol.* **1999,** *2–3*, 179–186.

45 Klug, H. P.; Alexander, L. X-ray Diffraction Procedures for Polycrystalline and Amorphous Materials (2nd ed.); Wiley: New York, **1974;** pp 618–709.

46 Misra, A.; Stein, R. S.; Chu, C.; Wilkes, G. L.; Desai, A. B. *J. Polym. Sci. Part C: Polym. Lett.* **1975,** *5*, 303–312.

47 Gosline, J. M.; Denny, M. W.; Demont, M. E. *Nature* **1984,** *309*, 551–552.

48 Elices, M.; Guinea, G. V.; Plaza, G. R.; Karatzas, C.; Riekel, C.; Agullo-Rueda, F.; Daza, R.; Perez-Rigueiro, J. *Macromolecules* **2011,** *5*, 1166–1176.

49 Elices, M.; Perez-Rigueiro, J.; Plaza, G. R.; Guinea, G. V. *JOM* **2005,** *2*, 60–66.

50 Plaza, G. R.; Corsini, P.; Perez-Rigueiro, J.; Marsano, E.; Guinea, G. V.; Elices, M. *J. Appl. Polym. Sci.* **2008,** *3*, 1793–1801.

51 Kaplan, D. L.; Lombardi, S.; Muller, W. S.; Fossey, S. A. Biomaterials. Novel Materials from Biological Sources; Stockton Press: New York, **1991;** p 53.

52 Perez-Rigueiro, J.; Viney, C.; Llorca, J.; Elices, M. *J. Appl. Polym. Sci.* **2000,** *10*, 1270–1277.

53 Madsen, B.; Shao, Z. Z.; Vollrath, F. *Int. J. Biol. Macromol.* **1999,** *2–3*, 301–306.

54 Marsh, R. E.; Corey, R. B.; Pauling, L. *Biochim. Biophys. Acta* **1955,** *1*, 1–34.

55 Yang, Z.; Grubb, D. T.; Jelinski, L. W. *Macromolecules* **1997,** *26*, 8254–8261.

56 Riekel, C.; Craig, C. L.; Burghammer, M.; Muller, M. *Naturwissenschaften* **2001,** *2*, 67–72.

57 Riekel, C.; Vollrath, F. *Int. J. Biol. Macromol.* **2001,** *3*, 203–210.

58 Grubb, D. T.; Ji, G. D. *Int. J. Biol. Macromol.* **1999,** *2–3*, 203–210.

59 Perez-Rigueiro, J.; Biancotto, L.; Corsini, P.; Marsano, E.; Elices, M.; Plaza, G. R.; Guinea, G. V. *Int. J. Biol. Macromol.* **2009,** *2*, 195–202.

60 Perez-Rigueiro, J.; Elices, M.; Plaza, G. R.; Guinea, G. V. *Macromolecules* **2007,** *15*, 5360–5365.

61 Termonia, Y. *Macromolecules* **1994,** *25*, 7378–7381.

62 Termonia, Y. Molecular modelling of the stress/strain behaviour of spider dragline. In Structural Biological Materials; Elices, M., Ed.; Pergamon Press: Amsterdam, **2000;** pp 335–349.

63 Buehler, M. J. *Nano Today* **2010,** *5*, 379–383.

64 Nova, A.; Keten, S.; Pugno, N. M.; Redaelli, A.; Buehler, M. J. *Nano Lett.* **2010,** *7*, 2626–2634.

65 Yin, J.; Chen, E.; Porter, D.; Shao, Z. Z. *Biomacromolecules* **2010,** *11*, 2890–2895.

66 Keten, S.; Xu, Z. P.; Ihle, B.; Buehler, M. J. *Nat. Mater.* **2010,** *4*, 359–367.

67 Keten, S.; Buehler, M. J. *J. R. Soc. Interface* **2010,** *53*, 1709–1721.

68 Simmons, A.; Michal, C.; Jelinski, L. *Science* **1996,** *5245*, 84.